Research paper

Synthesis of Cu-Cr-Fe ternary metal oxide nanocomposites with enhanced catalytic activity on the thermal decomposition of ammonium perchlorate

Gazi Hao*†, Lei Xiao*, Zhe Zhang*, Yubing Hu*, Jie Liu*, Hongbing Lei**, Fengqi Zhao***, Hongxu Gao***, and Wei Jiang*†

*School of Chemical Engineering, Nanjing University of Science and Technology, Nanjing 210094, CHINA
Phone: +86-25-84315042
†Corresponding author: hgznjust1989@163.com

**Shanxi North Xing'an Chemical Industry Co. Ltd, Taiyuan 030008, CHINA

***Science and Technology on Combustion and Explosion Laboratory, Xi'an Modern Chemistry Research Institute, Xi'an 710065, CHINA

Received: September 27, 2018 Accepted: March 15, 2019

Abstract

In this article, the Cu-Cr-Fe ternary metal oxide nanocomposites were synthesized by the co-precipitation method using $Cu(NO_3)_2{\cdot}3H_2O$, $Cr(NO_3)_3{\cdot}3H_2O$ and $Fe(NO_3)_3{\cdot}9H_2O$ as precursors, with PEG-400 act as a dispersant and ammonia as the precipitating agent. A variety of Cu-Cr-Fe ternary metal oxide nanocomposites with different molar ratios were obtained by keeping a constant amount of Cu and adjusting Cr/Fe molar ratios (Cr/Fe = 8:2, 6:4, 4:6 and 2:8). The crystal form and morphology of Cu-Cr-Fe ternary metal oxide nanocomposites were carried out by X-ray diffraction (XRD), energy dispersive X-ray spectroscopy (EDS), scanning electron microscopy (SEM) and transmission electron microscopy (TEM). The results show that the Cu-Cr-Fe ternary metal oxide nanocomposites mainly consist of $CuCr_2O_4$ and $CuFe_2O_4$, which are the good dispersing sphere particles with the average diameter of approximately 50 nm. Further, the catalytic effects of the Cu-Cr-Fe ternary metal oxide nanocomposites on the thermal decomposition of ammonium perchlorate (AP) were investigated by thermogravimetric analysis/differential scanning calorimetric (TG-DSC) techniques. Gratifyingly, the TG-DSC results that the four kinds of Cu-Cr-Fe ternary metal oxide nanocomposites have the significant catalytic effect for the thermal decomposition of AP, and the Cu-Cr-Fe ternary metal oxide nanocomposites with the molar ratio of Cu/Cr/Fe = 5:4:6 is verified to be the most efficient catalyst, which could lower the peak temperature of high-temperature decomposition of AP to 366.4 °C from 441.3 °C in the presence of 2%.

Keywords: Cu-Cr-Fe ternary metal oxide nanocomposites, co-precipitation, ammonium perchlorate, catalytic activity, thermal analysis

1. Introduction

Ammonium perchlorate (NH_4ClO_4, AP), with advantages of high oxygen content, relatively low price, has long been the main energy substance and outstanding oxidizer in composite solid propellants (CSPs), in which contains 60% to 80% AP[1)-5)]. Therefore, the burning behavior of CSPs is tightly relevant to the thermal decomposition of AP. The burning rate of CSPs can be increased by accelerating the thermal decomposition of AP. In general, there are two ways to enhance the thermal decomposition of AP. The first way is to reduce the particle size of AP. The second method is to use nanocatalysts instead of bulk catalysts. In fact, the addition of a small amount of nanocatalysts is the most common and effective treatment for improving the thermal decomposition of AP.

With the development of nanoscience and nanotechnology, nanocatalysts for enhancing the thermal

Table 1 Synthesis conditions of the Cu-Cr-Fe ternary metal oxide nanocomposites.

Samples	Cu/Cr/Fe ratios	Reaction temperature [°C]	Reaction time [h]	Calcination temperature [°C]	Calcination time [h]
S1	5:8:2	80	3	600	3
S2	5:6:4				
S3	5:4:6				
S4	5:2:8				

decomposition of AP have gained a great attention during the past decades, including nano-metals and nano-alloys (Fe, Co, Ni, Mg, Al, Cu, Zn, FeNi, NiCu, NiB, CoNi, NiMn, etc.)[6)−9)], nano-metal oxides and nano-metal composite oxides (Fe_2O_3, CuO, Cu_2O, PbO, CoO, Co_2O_3, TiO_2, NiO, Ni_2O_3, MnO_2, ZnO, CaO, MgO, CrO_3, Cr_2O_3, SnO_2, Bi_2O_3, V_2O_5, $CuO{\cdot}Fe_2O_3$, $CuO{\cdot}PbO$, $PbO{\cdot}SnO_2$, etc.)[10)−16)], nano-metal compounds and nano-metal hydroxides ($CaCO_3$, $PbCO_3$, $CuCr_2O_4$, $CuFe_2O_4$, $CoFe_2O_4$, $NiFe_2O_4$, FeC_2O_4, CuC_2O_4, CoC_2O_4, NiC_2O_4, $Cu(OH)_2$, $Cr(OH)_3$, $Al(OH)_3$, etc.)[17)−22)], nano-organic metal compounds (copper phthalate, lead phthalate, etc)[23),24)], nano-hydrogen storage materials (LiH, MgH_2, AlH_3, $LiBH_4$, $Mg(BH_4)_2$, Mg_2NiH_4, Mg_2CuH_3, etc)[25),26)] and nano-carbon materials (C, CB, C_{60}, carbon fiber, CNTs, GN, CNTs-based materials, GN-based materials, etc)[27)−33)]. Among the numerous nanocatalysts, nano copper chromite ($CuCr_2O_4$) has already been researched widely and been applied to the weapons, aerospace, and other areas of the defense industry.

In recent years, researches show the composite of different metal nanoparticles can combine the characteristics of different metals, and make up the scarcity of single metal, which can be attributed to the composite of two or more kinds of catalysts displaying synergetic effect[34)−36)]. Accordingly, taking into account the superiority of $CuCr_2O_4$, a lot of research work has been carried out about Cu-Cr composite metal oxides, such as Cu-Cr-O and Cu-Cr-Ti composite metal oxides[4),37),38)]. In our previous study, we present the preparation and characterization of the Cu-Cr-Pb ternary metal oxide nanocomposites. When the molar ratio of Cu/Cr/Pb = 4:10:1, the Cu-Cr-Pb ternary metal oxide nanocomposites have good dispersion, and more effective catalytic performance for AP, which could display the synergetic effect of Cu, Cr and Pb[39)].

Herein, we present a simple co-precipitation route to for the synthesis of the uniform Cu-Cr-Fe ternary metal oxide nanocomposites. The structure, size and catalytic properties of the Cu-Cr-Fe ternary metal oxide nanocomposites with different molar ratios on the thermal decomposition of AP are further investigated in details.

2. Experimental section

2.1 Synthesis of Cu-Cr-Fe ternary metal oxide nanocomposites

All chemicals were of analytical purity and used as received without further purification. All syntheses were conducted under the same experimental conditions except for the different Cr/Fe molar ratios (see Table 1). Samples composed of Cr/Fe with molar ratios of 8:2, 6:4, 4:6, and 2:8 were marked as S1, S2, S3 and S4, respectively. The reactions for the synthesis of Cu-Cr-Fe ternary metal oxide nanocomposites can be described as follow equations:

$$Cu^{2+}+2OH^{-}=Cu(OH)_2\downarrow \quad (1)$$

$$Cr^{3+}+3OH^{-}=Cr(OH)_3\downarrow \quad (2)$$

$$Fe^{3+}+3OH^{-}=Fe(OH)_3\downarrow \quad (3)$$

$$Cu(OH)_2+Cr(OH)_3+Fe(OH)_3\rightarrow CuO+Cr_2O_3+Fe_2O_3\rightarrow CuCr_2O_4/CuFe_2O_4 \quad (4)$$

In a typical procedure of S1, 0.01 mol $Cu(NO_3)_2{\cdot}3H_2O$, 0.016 mol $Cr(NO_3)_3{\cdot}9H_2O$ and 0.004 mol $Fe(NO_3)_2{\cdot}9H_2O$ were dissolved in 100 mL of ethanol aqueous solution (V/V=1:1) to form a homogeneous metal nitrate solution, in which 2% of polyethylene glycol 400 (PEG-400) was added as a dispersant. Then, the solution was transferred to a 250 mL three-necked flask and heated to 40 °C for 1 h in a water bath. Subsequently, the ammonia was added dropwise to the solution over 30 min and with continuous stirring and the pH of the solution was set to approximately 7.0. After that, precipitation had occurred and the solution was stirred continuously for 3 h at 80 °C. The resultant precipitates were washed several times with ethanol and deionized water alternately, and gathered by centrifugation and then further calcined in air atmosphere at 600 °C for 3 h. Finally, the products were treated by a slight grinding, which yielded the Cu-Cr-Fe (S1, Cu/Cr/Fe =5:8:2) nanocomposites. Similarly, the other Cu-Cr-Fe ternary metal oxide nanocomposites with different Cr/Fe molar ratios could be obtained.

2.2 Preparation of the mixtures of AP and Cu-Cr-Fe ternary metal oxide nanocomposites

The mixtures of AP (D_{50} = 64μm) and Cu-Cr-Fe ternary metal oxide nanocomposites were prepared by ultrasonic-assisted grinding method. 0.02 g of Cu-Cr-Fe ternary metal oxide nanocomposites was added into 3 mL of ethyl acetate solution with ultrasonic stirring for 5 min to form a suspension. Then, 0.98 g of AP was slowly added into the suspension. After ultrasonic stirring over 5 min, the mixtures were transferred into the agate mortar and further homogenized by a slight grinding. When the majority of ethyl acetate solution was evaporated, the mixtures were dried at 50 °C in drying oven. Finally, the mixtures of AP and Cu-Cr-Fe ternary metal oxide nanocomposites were obtained.

2.3 Characterization

The structures of the products were examined by X-ray powder diffraction using a Bruker D8-Advanced

diffractometer in the 2θ range of 20°–80° with Cu Kα_1 radiation ($\lambda = 0.15406$ nm) operated at 40 kV and 40 mA. The size and morphology of Cu-Cr-Fe ternary metal oxide nanocomposites were observed by a field emission scanning electron microscope (FE-SEM, Hitachi S-4800 Ⅱ) operating at 15 kV and transmission electron microscopy (TEM, Tecnai 12) with an acceleration voltage of 200 kV, respectively. The surface chemical compositions of Cu-Cr-Fe ternary metal oxide nanocomposites were analyzed by energy dispersive X-ray spectrometric microanalysis (EDS).

2.4 Measurement of the catalytic activity of Cu-Cr-Fe ternary metal oxide nanocomposites

To examine the catalytic activity of as-prepared Cu-Cr-Fe ternary metal oxide nanocomposites, thermogravimetric (TG) analysis and differential scanning calorimetric (DSC) techniques were applied to investigate the thermal decomposition of the mixtures of AP and Cu-Cr-Fe ternary metal oxide nanocomposites using a SDT Q600 thermal analyzer at different heating rates of 5–20 °C min^{-1} from 50 to 500 °C with nitrogen flow rate of 20 mL min^{-1}. The Cu-Cr-Fe ternary metal oxide nanocomposites and AP were mixed with the mass ratio of 2:98. For a comparison, pure AP was also put into the measurement. In addition, the effect of content of Cu-Cr-Fe ternary metal oxide nanocomposites on the thermal decomposition of AP was also studied.

3. Results and discussion

3.1 The structure and morphology of Cu-Cr-Fe ternary metal oxide nanocomposites

The structures of Cu-Cr-Fe ternary metal oxide nanocomposites were characterized by XRD. The XRD patterns (Figure 1) show the as-prepared Cu-Cr-Fe ternary metal oxide nanocomposites are constituted with spinel $CuCr_2O_4$ and $CuFe_2O_4$. The diffraction data are in good agreement with JCPDS cards of $CuCr_2O_4$ (JCPDS 34-0424) and $CuFe_2O_4$ (JCPDS 25-0283), respectively[40),41)]. With decrement of Cr/Fe molar ratios, the intensities of major peaks of $CuCr_2O_4$ decrease, while the intensities of major peaks of $CuFe_2O_4$ increase. According to XRD analysis, Cu-Cr-Fe ternary metal oxide nanocomposites contain a small amount of CuO, Cr_2O_3, and Fe_2O_3. The wide diffraction peaks of samples indicate that the Cu-Cr-Fe ternary metal oxide nanocomposites have a small particle size.

In addition, the chemical compositions of the Cu-Cr-Fe ternary metal oxide nanocomposites were measured by energy dispersive X-ray spectrometric microanalysis. It showed that S1-S4 samples are composed of Cu, Cr, Fe and O (Figure 2).

The atomic ratios of Cu/Cr/Fe for S1-S4 samples are listed in Table 2, which confirms that there is almost no element loss during the preparation process.

The morphology and size of Cu-Cr-Fe ternary metal oxide nanocomposites were observed by FE-SEM and TEM. As shown in Figure 3, all of Cu-Cr-Fe ternary metal oxide nanocomposites have an average size of

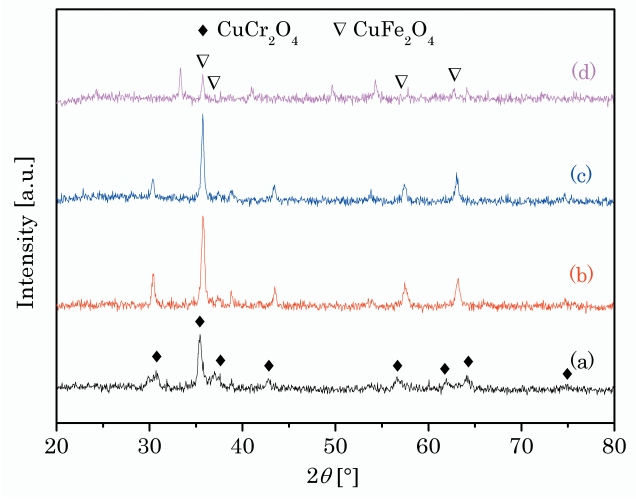

Figure 1 XRD patterns of (a) S1, (b) S2, (c) S3 and (d) S4.

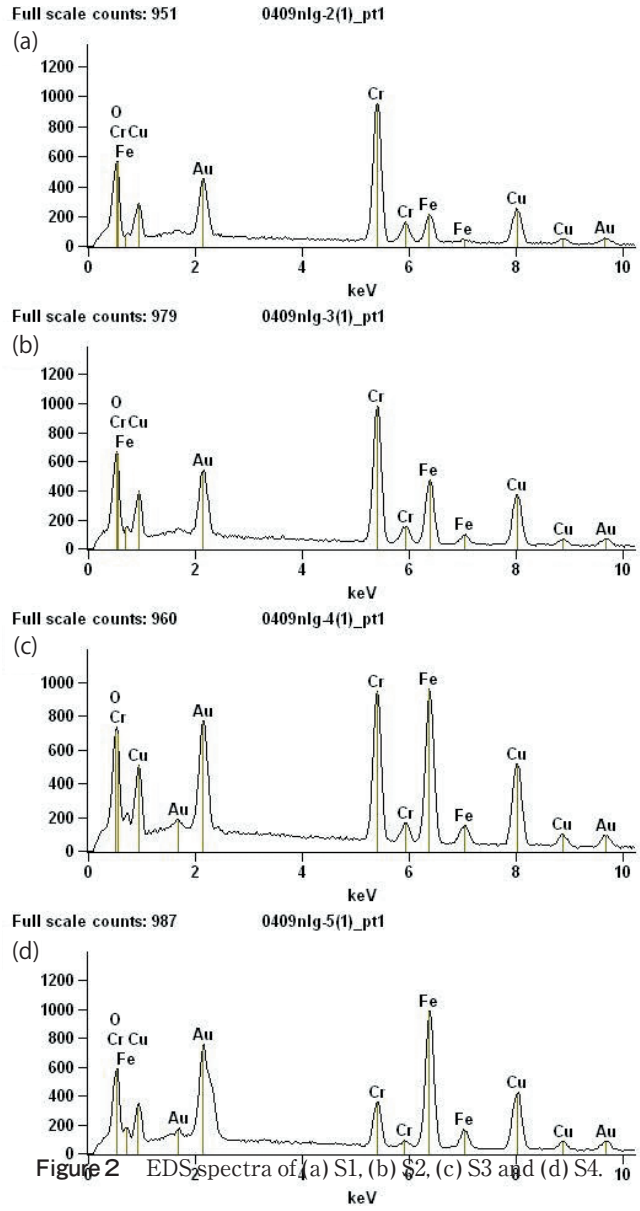

Figure 2 EDS spectra of (a) S1, (b) S2, (c) S3 and (d) S4.

Table 2 The atomic ratios of Cu/Cr/Fe for S1-S4 samples.

Samples	Cu/Cr/Fe ratios (theoretical value)	Cu/Cr/Fe ratios (measured value)
S1	5:8:2	5:8.23:2.04
S2	5:6:4	5:6.33:4.01
S3	5:4:6	5:4.16:5.82
S4	5:2:8	5:1.86:7.73

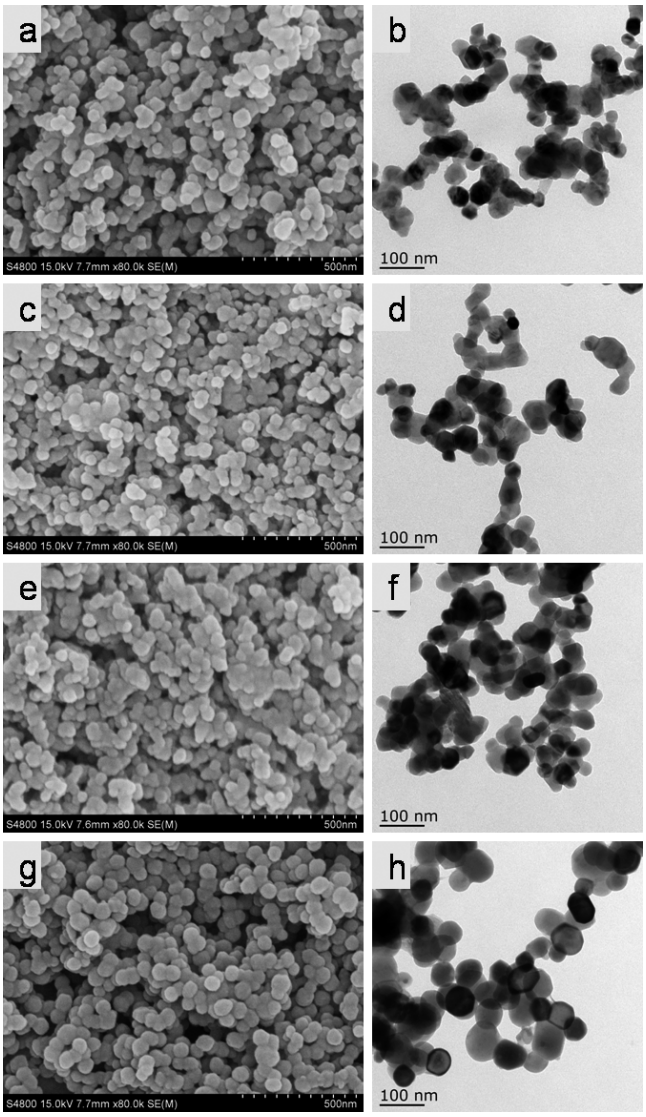

Figure 3 Representative SEM images (a, c, e and g) and TEM images (b, d, f and h) of Cu–Cr–Fe ternary metal oxide nanocomposites of S1 (a and b), S2 (c and d), S3 (e and f) and S4 (g and h).

approximately 50 nm with a narrow size distribution and a spherical shape.

According to the above analysis results, the Cu-Cr-Fe ternary metal oxide nanocomposites with various atomic ratios of Cu/Cr/Fe and mean particle size of 50 nm were successfully prepared by the co-precipitation method.

3.2 Catalytic activity of Cu-Cr-Fe ternary metal oxide nanocomposites

To evaluate the catalytic activity of the Cu-Cr-Fe ternary metal oxide nanocomposites, the thermal

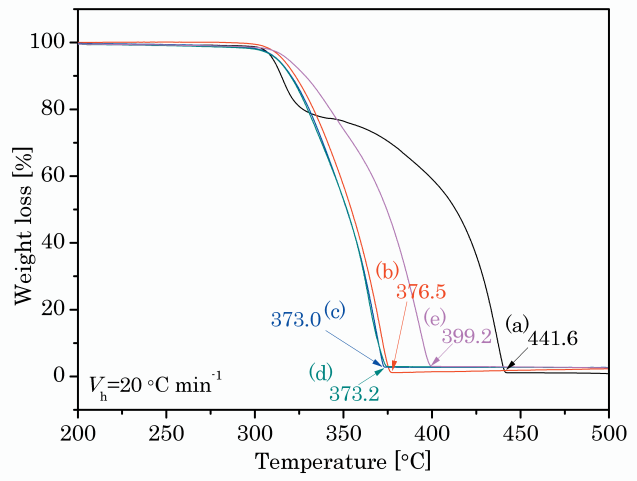

Figure 4 TG curves for the decomposition of (a) AP, (b) S1/AP, (c) S2/AP, (d) S3/AP and (e) S4/AP.

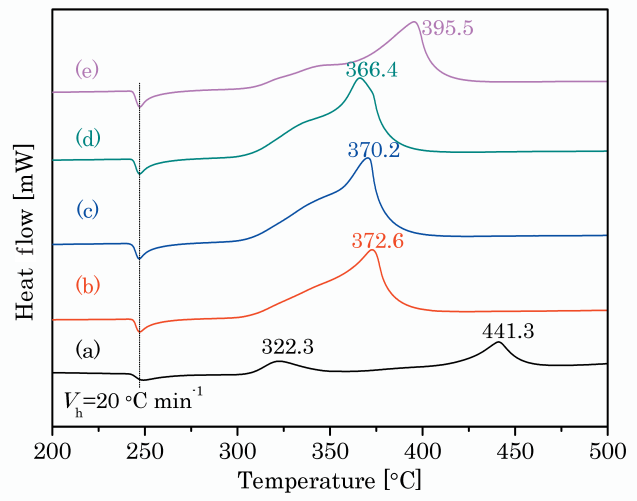

Figure 5 DSC curves for the decomposition of (a) pure AP, (b) S1/AP, (c) S2/AP, (d) S3/AP and (e) S4/AP.

decomposition of the mixtures of AP and Cu-Cr-Fe ternary metal oxide nanocomposites were studied. The TG and DSC curves of the thermal decomposition of AP and the mixtures of S1-S4/AP are shown in Figures 4 and 5, respectively.

Figure 4 shows the TG curves of AP and the mixtures of S1-S4/AP samples. It is obvious that only one weight loss was detected in AP and two weight losses were detected in S1-S4/AP samples, while the mixtures have much lower decomposition temperatures. These findings agree well with the DSC results. Figure 5 shows the DSC curves of AP and the mixtures of S1-S4/AP samples. For the pure AP, an endothermic process was located about 247 °C due to the crystallographic transformation of AP from orthorhombic to cubic without weight loss[42),43)]. With the increase of the temperature, there are two exothermic processes for pure AP, which is followed by two exothermic peaks. The peak temperature of low temperature decomposition peak (T_L) at 322.3 °C is due to the low-temperature decomposition (LTD) of AP, during which AP partially decomposes to generate some gaseous products. At higher temperature, the peak temperature of high temperature decomposition peak (T_H) which located

at 441.3 °C is attributable to high-temperature decomposition (HTD) of AP, arising from the full conversion of AP to gaseous products.

For the mixtures of S1-S4/AP samples, the same endothermic peaks at 247 °C were also found, which suggest that the S1-S4 nanocomposites have no significant influences on the phase transition of AP. Upon addition of S1, the T_H of AP was decreased by 68.7 °C and the low-temperature decomposition peak weakened, suggesting the apparent catalytic effect of Cu-Cr-Fe ternary metal oxide nanocomposites on the decomposition of AP. More interestingly, when Cu/Cr/Fe molar ratio was 5:4:6 to form S3, it was found that S3 could reduce the T_H of AP by 74.9 °C from 441.3 °C to 366.4 °C, indicating that S3 shows better catalytic performance on the decomposition of AP in comparison with others. However, Cu-Cr-Fe ternary metal oxide nanocomposites with a molar ratio of Cu/Cr/Fe=5:2:8 exhibited the worst catalytic effect among all of Cu-Cr-Fe ternary metal oxide nanocomposites. Therefore, Cu-Cr-Fe ternary metal oxide nanocomposites with a molar ratio of Cu/Cr/Fe=5:4:6 show synergetic effect.

Additionally, the DSC data of AP and the mixtures of S1 -S4/AP are shown in Table 3. From Table 3, the apparent decomposition heat of AP was 941 Jg^{-1}. The apparent decomposition heats of S1-S4/AP samples were detected to be 1739, 1820, 1868 and 1699 Jg^{-1}, respectively. Surprisingly, the apparent decomposition heat of S3/AP reached to 1868 J g^{-1} with a highest growth rate of 98.5% compared with pure AP. It shows once again that Cu-Cr-Fe ternary metal oxide nanocomposites prepared with a molar ratio of Cu/Cr/Fe=5:4:6 have an optimal catalytic effect on the decomposition of AP.

At present, it is well known that a scheme of thermal decomposition of ammonium perchlorate as a version of proton mechanism proposed by Jackobs can be presented as follow[42]:

$$NH_4^+ + ClO_4^- = NH_3(a) + HClO_4(a) = NH_3(g) + HClO_4(g) \quad (5)$$

The most essential feature of the thermal decomposition of AP is the two stages decomposition, low temperature decomposition, and high temperature decomposition commonly referred as LTD and HTD, respectively[40]. At first, a proton passing from the ammonium ion to perchlorate ion becomes mobile and then the gaseous NH_3 and $HClO_4$ formed. At low temperature (< 350°C), the gaseous NH_3 and $HClO_4$ incompletely reacted to generate N_2O, O_2, Cl_2 and H_2O, the residual NH_3 is adsorbed on the surface of AP. Subsequently, NO, O_2, Cl_2 and H_2O were formed at the high-temperature (> 350°C) decomposition step of AP[14]. However, the decomposition behavior of AP will be different with the help Cu-Cr-Fe ternary metal oxide nanocomposites as compared to the pure AP. According to the experimental results, Cu-Cr-Fe ternary metal oxide nanocomposites have a slight influence on the low-temperature decomposition step of AP because the decomposition stops when the residual NH_3 is totally adsorbed on the surface of AP[42),44]. Fortunately, Cu-Cr-Fe ternary metal oxide nanocomposites have a significant effect on the high-temperature decomposition step of AP due to the high proton conductivity of Cu-Cr-Fe ternary metal oxide nanocomposites arising from their nature of semiconductor and their positive holes and the corresponding active sites for the adsorption of gaseous products as well as the synergistic effect caused by Cu, Cr and Fe salts[45),46].

Table 3 DSC data of AP and the mixtures of S1-S4/AP.

Samples	T_L [°C]	T_H [°C]	H [J g^{-1}]	ΔH [J g^{-1}]
AP	322.3	441.3	941	—
S1/AP	—	372.6	1739	798
S2/AP	—	370.2	1820	879
S3/AP	—	366.4	1868	927
S4/AP	—	395.5	1699	758

Table 4 The T_p (°C) of AP and the mixtures of S1-S4/AP at different heating rates.

Samples	5 [°C min^{-1}]	10 [°C min^{-1}]	15 [°C min^{-1}]	20 [°C min^{-1}]
AP	408.1	419.6	430.2	441.3
S1/AP	344.7	360.4	368.8	372.6
S2/AP	344.0	355.9	363.6	370.2
S3/AP	343.5	355.7	363.2	366.4
S4/AP	366.6	378.3	387.6	395.5

Table 5 The kinetic parameters for HTD of AP and the mixtures of S1-S4/AP.

Samples	E_a [kJ·mol^{-1}]	A [min^{-1}]	k [s^{-1}]
AP	156.7	2.31×10^{11}	2.67×10^{-3}
S1/AP	149.6	1.02×10^{12}	4.18×10^{-2}
S2/AP	165.5	2.71×10^{13}	6.49×10^{-2}
S3/AP	182.6	8.26×10^{14}	9.40×10^{-2}
S4/AP	160.0	2.88×10^{12}	1.83×10^{-2}

The kinetic parameters for AP decomposition can be calculated according to the exothermic peak temperature dependence as a function of heating rate (Kissinger correlation) and Arrhenius equation (Equation (6) and Equation (7))[47]:

$$\ln\left(\frac{\beta}{T_p^2}\right) = -\frac{E_a}{RT_p} + \ln\left(\frac{AR}{E_a}\right) \quad (6)$$

$$k = A \cdot \exp\left(-\frac{E_a}{RT_p}\right) \quad (7)$$

Where β is the heating rate in degrees Celsius per minute, T_p is the maximum peak temperature, R is the ideal gas constant, E_a is the activation energy, A is the frequency factor, and k is the reaction rate constant when the T is equal to 673.15 K. The T_p of AP and the mixtures of S1-S4/AP at different heating rates are shown in Table 4 and the kinetic parameters for HTD of AP and the mixtures of S1-S4/AP are shown in Table 5.

As shown in Table 5, the k value of AP is 2.67×10^{-3} s^{-1}. Upon the addition of 2 % of S1-S4, the reaction rate constants (k values) for HTD of S1/AP, S2/AP, S3/AP and S4/AP samples have been significantly increased to 4.18×10^{-2} s^{-1}, 6.49×10^{-2} s^{-1}, 9.40×10^{-2} s^{-1} and 1.83×10^{-2}

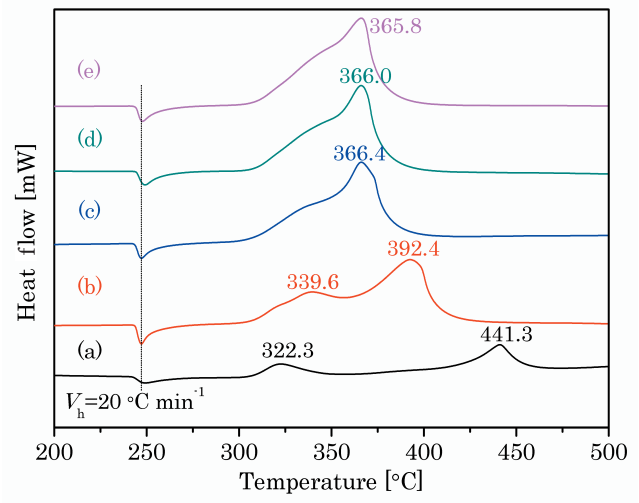

Figure 6 DSC curves for the decomposition of S3/AP samples with different contents of S3: (a) 0, (b) 1%, (c) 2%, (d) 3% and (e) 4%.

Table 6 The influence of the content of S3 on the apparent decomposition heat of S3/AP samples.

Samples	T_L [°C]	T_H [°C]	H [J g^{-1}]	ΔH [J g^{-1}]
AP	322.3	441.3	941	—
1 %S3/AP	339.6	392.4	1827	886
2 %S3/AP	—	364.4	1868	927
3 %S3/AP	—	366.0	1802	861
4 %S3/AP	—	365.8	1829	888

s^{-1} from 2.67×10^{-3} s^{-1}, respectively. The high k value can be attributed to easy facilitation of the decomposition reaction, which clearly indicates enhanced catalytic activity in the presence of S3.

To explore the effect of content of the as-prepared Cu-Cr-Fe ternary metal oxide nanocomposites on the thermal decomposition of AP, the thermal decomposition of AP and 1−4% of S3 were examined. Figure 6 shows the DSC curves of AP and 1−4% of S3. As shown in Figure 6, with increasing content of S3, the exothermic peak temperature of S3/AP gradually decreased. When the contents of S3 are 1%, 2%, 3% and 4%, the peak temperatures of HTD of S3/AP were 392.4 °C, 366.4 °C, 366.0 °C and 365.8 °C, respectively. However, the change of contents had insignificantly influence on the thermal decomposition of S3/AP, especially when the content of S3 is more than 2 %. The apparent decomposition heats of S3/AP samples are presented in the Table 6, which increased first and then decreased as the increasing content of S3. Thus, the optimal content of S3 for accelerating the thermal decomposition of AP is approximately 2%.

4. Conclusions

In summary, the Cu-Cr-Fe ternary nanocomposites were prepared by the co-precipitation method. The Cu-Cr-Fe ternary metal oxide nanocomposites are composed of $CuCr_2O_4$ and $CuFe_2O_4$, which show good dispersing sphere particles with the average size of approximately 50 nm. The DSC/TG results indicate that the thermal decomposition of AP was significantly enhanced by Cu-Cr-Fe ternary metal oxide nanocomposites. At the best conditions, the Cu-Cr-Fe ternary metal oxide nanocomposites had a molar ratio of Cu/Cr/Fe = 5:4:6 and the usage amount of Cu-Cr-Fe ternary metal oxide nanocomposites was 2%. Hence, there is much potential for the use of Cu-Cr-Fe ternary metal oxide nanocomposites in catalytic decomposition of AP.

Acknowledgements

This work was financially supported by the National Natural Science Foundation of China (Grant Nos. 21805139 and 51606102), the Fundamental Research Funds for the Central Universities (Grant No. 30918011312), Youth Scientific and Technological Innovation Project (Grant No. QKCZ201713) and Nanjing University of Science and Technology.

References

1) S. Chaturvedi and P.N. Dave, J. Saudi. Chem. Soc., 17, 135−149 (2013).
2) C.W. Wu, K. Sullivan, S. Chowdhury, G.Q. Jian, L. Zhou, and M.R. Zachariah, Adv. Funct. Mater., 22, 78−85 (2012).
3) F.S. Li, W. Jiang, J. Liu, X.D. Guo, Y.J. Wang, and G.Z. Hao, "Chapter five-applications of nanocatalysts in solid rocket propellants, in: energetic nanomaterials", Elsevier, Amsterdam (2016).
4) S.G. Hosseini, M.A. Alavi, A. Ghavi, S.J.H. Toloti, and F. Agend, J. Therm. Anal. Calorim., 119, 99−109 (2014).
5) X.L. Song, Y. Wang, D. Song, C.W. An, and J.Y. Wang, Sci. Tech. Energetic Materials, 77, 65−71 (2017).
6) G. Singh, S.K. Sengupta, I.P.S. Kapoor, S. Dubey, R. Dubey, and S. Singh, J. Energ. Mater., 31, 165−177 (2013).
7) Y. Nishiwaki, T. Matsunaga, and M. Kumasaki, Sci. Tech. Energetic Materials, 79, 15−21 (2018).
8) L.L. Liu, F.S. Li, L.H. Tan, L. Ming, and Y. Yi, Propellants, Explos., Pyrotech., 29, 34−38 (2004).
9) R. Dubey, M. Chawla, P.F. Siril, and G. Singh, Thermochim. Acta., 572, 30−38 (2013).
10) Z.Y. Ma, F.S. Li, and H.P. Bai, Propellants, Explos., Pyrotech., 31, 447−451 (2006).
11) Y.Y. Xu, D.R. Chen, M.L. Jiao, and K.Y. Xue, Mater. Res. Bull., 42, 1723−1731 (2007).
12) M.H. Habibi and F. Fakhri, J. Therm. Anal. Calorim., 115, 1329−1333 (2014).
13) Y.P. Wang, X.Y. Xia, J.W. Zhu, Y. Li, X. Wang, and X.D. Hu, Combust. Sci. Technol., 183, 154−162 (2010).
14) S. Chaturvedi and P.N. Dave, J. Exp. Nanosci., 7, 205−231 (2012).
15) I.P.S. Kapoor, P. Srivastava, and G. Singh, Propellants, Explos., Pyrotech., 34, 351−356 (2009).
16) Z. Ge, X. Li, W.G. Zhang, Q.L. Sun, C.P. Chai, and Y.J. Luo, J. Solid State Chem., 258, 138−145 (2018).
17) G. Singh, I.P.S. Kapoor, S. Dubey, and P.F. Siril, Propellants, Explos., Pyrotech., 34, 72−77 (2009).
18) S. Singh, P. Srivastava, and G. Singh, J. Ind. Eng. Chem., 27, 88−95 (2015).
19) Y.W. Lu, Y.F. Zhu, P.F. Xu, P. Ye, B. Gao, Y. Sun, and C.P. Guo, J. Solid State Chem., 258, 718−721 (2018).
20) W.J. Zhang, P. Li, H.B. Xu, R.D. Sun, P.H. Qing, and Y. Zhang, J. Hazard. Mater., 268, 273−280 (2014).

21) X. Zheng, P. Li, S. Zheng, and Y. Zhang, Powder Technol., 268, 446−451 (2014).
22) G.Z. Hao, J. Liu, Q.E. Liu, L. Xiao, X. Ke, H. Gao, P. Du, W. Jiang, F.Q. Zhao, and H.X. Gao, Propellants, Explos., Pyrotech., 42, 947−952 (2017).
23) G.Z. Hao, J. Liu, H. Gao, L. Xiao, X. Ke, W. Jiang, F.Q. Zhao, and H.X. Gao, Propellants, Explos., Pyrotech., 40, 848−853 (2015).
24) W.Y. Zhao, T.L. Zhang, N.M. Song, L.N. Zhang, Z.K. Chen, L. Yang, and Z.N. Zhou, RSC Adv., 6, 71223−71231 (2016).
25) L.L. Liu, J. Li, L.Y. Zhang, and S.Y. Tian, J. Hazard. Mater., 342, 477−481 (2018).
26) X.Y. Ding, Y.J. Shu, H.T. Xu, and Z.Q. Chen, Propellants Explos. Pyrotech., 43, 267−273 (2018).
27) F. Wu, X.D. Guo, Z.P. Jiao, L. Li, H.Y. Lin, and Z.X. Wang, Chinese J. Energ. Mater., 24, 261−268 (2016).
28) P. Cui and A.J. Wang, J. Saudi. Chem. Soc., 20, 343−348 (2016).
29) Y.F. Zhang, X.H. Liu, J.R. Nie, L. Yu, Y.L. Zhong, and C. Huang, J. Solid State Chem., 184, 387−390 (2011).
30) N. Li, Z.F. Geng, M.H. Cao, L. Ren, X.Y. Zhao, B. Liu, Y. Tian, and C.W. Hu, Carbon. 54, 124−132 (2013).
31) S.G. Hosseini, Z. Khodadadipoor, and M. Mahyari, Appl. Organomet. Chem., 32, e3959 (2018).
32) S. Isert, L. Xin, J. Xie, and S.F. Son, Combust. Flame. 183, 322−329 (2017).
33) N.K. Memon, A.W. McBain, and S.F. Son, J. Propul. Power. 32, 682−686 (2016).
34) R. Li, X.X. Liu, Y.C. Huang, and X.J. Wang, J. Solid Rocket Technol., 31, 607−611 (2008).
35) S.G. Hosseini and R. Abazari, RSC Adv., 5, 96777−96784 (2015).
36) D.C.K. Rao, N. Yadav, and P.C. Joshi, Defence Technol., 12, 297−304 (2016).
37) P.S. Sathiskumar, C.R. Thomas, and G. Madras, Ind. Eng. Chem. Res., 51, 10108−10116 (2012).
38) W. Li and H. Cheng, Solid State Sci., 9, 750−755 (2007).
39) G.Z. Hao, J. Liu, H.H. Liu, L. Xiao, Y. Qiao, H. Gao, W. Jiang, and F.Q. Zhao, J. Therm. Anal. Calorim., 123, 263−272 (2016).
40) S.G. Hosseini, R. Abazari, and A. Gavi, Solid State Sci., 37, 72−79 (2014).
41) A. Phuruangrat, B. Kuntalue, S. Thongtem, and T. Thongtem, Mater. Lett., 167, 65−68 (2016).
42) V.V. Boldyrev, Thermochim. Acta. 443, 1−36 (2006).
43) Z.G. Jia, D.P. Ren, Q.Z. Wang, and R.S. Zhu, Appl. Surf. Sci., 270, 312−318 (2013).
44) T.D. Hedman and M.L. Gross, Propellants, Explos., Pyrotech., 41, 254−259 (2016).
45) P.R. Patil, V.N. Krishnamurthy, and S.S. Joshi, Propellants Explos., Pyrotech., 33, 266−270 (2008).
46) X.L. Xu, W.K. Chen, and J.Q. Li, J. Mol. Structheochem., 860, 18−23 (2008).
47) R.L. Blaine and H.E. Kissinger, Thermochim. Acta., 540, 1−6 (2012).